Form Factors of Block Copolymer Micelles with Excluded-Volume Interactions of the Corona Chains Determined by Monte Carlo Simulations

Carsten Svaneborg*,† and Jan Skov Pedersen‡

Condensed Matter Physics and Chemistry Department, Risø National Laboratory, DK-4000 Roskilde, Denmark

Received June 19, 2001; Revised Manuscript Received October 18, 2001

ABSTRACT: The scattering of a diblock copolymer micelle has been simulated using Monte Carlo techniques. The scattering is analyzed using a novel model, where the corona is represented as a dilute/semidilute polymer solution with a radial profile. This approach decouples the scattering due to interaction and connectivity induced density fluctuations and scattering due to the radial profile of the corona. Three different profiles have been used to fit the simulated corona scattering: a box with a Gaussian tail and two maximum entropy (ME) profiles; chain penetration into the core region is not allowed for any of the profiles. Excellent fits are obtained, especially for a ME profile with three parameters. An excluded-volume parameter and the corona compressibility are obtained and show a strong dependence on surface coverage. The derived expressions for the form factor provides a new approach for analyzing experimental data obtained by neutron or X-ray small-angle scattering for block copolymer micelles with significant intra- and interchain excluded-volume interactions.

1. Introduction

When a diblock copolymer is dissolved in a solvent that is good for one block and bad for the other block, micelles are spontaneously formed. These micelles have a relatively dense core of the insoluble blocks surrounded by a diffuse corona consisting of the solvated blocks. The core can have various geometric shapes such as spherical, elliptical, or cylindrical, depending on solvent and the length of the polymer blocks.[1] Such micelles provide a model system for studying the interactions between polymer chains tethered to a curved surface.[2,3]

Much work have been invested in understanding properties of such systems, as tethering polymers to a surface provide a way of modifying the physical, chemical, and biological properties.[4,5] There are numerous studies in the literature of polymers tethered to a flat interface forming a polymer layer; see e.g. refs 6−9. For chains tethered to a convex surface such as a sphere the available volume per chain segment will grow rapidly for segments far from the first segment, which is tethered to the surface, and this has a strong effect on the properties of the polymer layer. The profiles of brushes on convex surface have been examined using variational minimization of mean field theory,[10] self-consistent-field theory,[2,3,11,12,] and simulation techniques such as Monte Carlo and molecular dynamics simulations.[13,14]

Under good solvent conditions a reduced surface coverage of a flat polymer layer can be defined as $\sigma = \pi R_{g0}^2/A'$, where R_{g0} is the radius of gyration of an unperturbed polymer chain and A' is the surface area available per chain (the inverse grafting density). For $\sigma \ll 1$ (the mushroom regime) all chains are essentially isolated. The polymer layer will be laterally inhomogeneous, and the conformation of a single polymer chain depends only on self-interactions and the presence of the surface. The profile of a polymer layer has recently been investigated by a renormalization group calculation in the low coverage limit.[15] For $\sigma \gg 1$ (the brush regime) each chain will interact with many neighboring chains, and chains will stretch away from the surface in an attempt to reduce the excluded-volume energy contribution by a reduction of the monomer density, which is achieved by increasing the height of the polymer layer. However, chain stretching will be accompanied by a decrease in the configurational entropy caused by the reduction of the number of possible chain configurations. The height of the polymer layer is determined by the balance of these two effects. In the brush regime the layer will be laterally homogeneous, and the chain stretching will be uniform except at the outer edge of the layer, where there will be some fluctuations due to the increased degrees of freedom of the chain ends.[10]

For a spherical micellar core we define specifically the reduced surface coverage as

$$\sigma = \frac{N\pi {R_{g0}}^2}{4\pi(R_{co} + R_{g0})^2} \tag{1}$$

Here R_{g0} is the unperturbed radius of gyration of the chains, while R_{co} is the core radius, and N is the number of chains. The reduced surface coverage is the packing fraction of chains on the surface, assuming that chains are spherical objects on the surface of the core. Because of the nonpenetration of the chains into the core region, the center-of-mass of a chain is displaced a distance about R_{g0} from the core surface, yielding an effective surface area per chain of $4\pi(R_{co} + R_{g0})^2/N$, while the cross-sectional area of a chain is $\pi {R_{g0}}^2$.

The topic of the present article is to present results from computer simulations for the scattering from micelles as well as an analysis of the results obtained

† Present address: Max-Planck-Institute for Polymer Research, Theory Group, PO Box 3148, D-55021 Mainz, Germany.

‡ Present address: Department of Chemistry, University of Aarhus, Langelandsgade 140, DK-8000 Aarhus C, Denmark.

10.1021/ma011046v CCC: $22.00
Published on Web 12/27/2001

by a novel semiempirical model. The model is a generalization of core−shell models that takes the scattering due to density fluctuation into account. The model allows the radial profile, chain radius of gyration, and the corona osmotic compressibility to be obtained from micellar scattering data.

We have performed simulations of the scattering for surface coverages $\sigma < 5$, which correspond to the region of surface coverages experimentally available for copolymer micelles; see e.g. refs 2, 16, and 17. The computer simulations have been performed using semiflexible chains with excluded-volume interactions, where chains are excluded from the spherical core region. Monte Carlo simulation techniques (MC) allow us to sample the scattering contributions from the micelle just as in a real experiment using contrast variation techniques, but using a well-defined model for the scattering object, here a micelle. This allows us to test models for the scattering from complex objects using simulation results, and it allows us to correlate the observed scattering to properties of the simulated model system, which will improve the interpretation of experimental scattering data. The simulation results are analyzed using a semiempirical model, which combines expressions for the scattering from a core−shell model with that of a dilute/semidilute polymer solution; a similar model have been used by de Gennes for describing the dynamics of brushes at flat interfaces.[18,19] We have used three radial profiles for describing the average radial profile, a box with a Gaussian tail, and two maximum entropy profiles,[20−22] where knowledge of the two or three first momenta of the profile is assumed.

The paper is organized as follows: In section 2 we present a derivation of the model; section 3 presents the Monte Carlo simulations and the quantities that are sampled during the MC simulations. In section 4 our MC data are presented and discussed, while section 5 contains our analysis and modeling of the data; our conclusions are summarized in section 6.

2. Analytical Models

In a dilute polymer solution polymers are well-separated, and as a result, the conformation and position of different polymer chains are uncorrelated. The scattering from the solution is given by the single chain form factor, which for an ideal flexible chain is given by $F_{\mathrm{Debye}}(x) = 2[x - 1 + \exp(-x)]/x^2$ with $x = (qR_g)^2$, where R_g is the radius of gyration and q the magnitude of the scattering vector.[23] For $qR_g \gg 1$ the form factor follows a $(qR_g)^{-2}$ power law; this is a reflection of the $\sqrt{\langle R_{ij}^2 \rangle} \propto |i - j|^2$ scaling relation between the root-mean-square (rms) distance between two sites on the chain and the contour length of the chain segments connecting the two sites. Topologically, the ideal chain is a connected stringlike object with a fractal dimension of two, while actual polymer chains are multiscale fractals due to their finite size and the semiflexibility of the polymer backbone.

The reduced density for an ordinary polymer solution is defined as $\Sigma = 4\pi R_{g0}^3\rho/3$ (identical to the reduced overlap concentration c/c^*, where c^* is the overlap concentration of a polymer solution), and ρ is the number density of chains. If the reduced density is well below unity, the solution is dilute, and polymers are well-separated. If the reduced density is well above unity, the solution is in the semidilute regime, where polymers are entangled, forming a transient network of intermeshed chains.[24,25] Using a discrete model with n sites per chain, the scattering from a semidilute solution follows the predictions from PRISM theory,[26,27] which states that it depends on the single-chain scattering and a direct interchain correlation function $c(q)$ as

$$F_{\mathrm{PRISM}}(q) = \frac{F_{\mathrm{Debye}}(q)}{1 - n\rho c(q)\, F_{\mathrm{Debye}}(q)} \tag{2}$$

Here we have neglected the effects of self-avoidance, and we do therefore not consider the screening at higher concentrations. Let us assume that the direct correlation function can be approximated by its low-q limit; then $-n\rho c(q)$ can be approximated by an effective concentration-dependent excluded-volume interaction parameter $\nu(\Sigma)$.[27] This turns the PRISM expression into the form of a random phase approximation (RPA).[28] Defining the reduced surface compressibility as $\kappa \equiv \partial\Pi^*/\partial\Sigma$, where the reduced osmotic pressure is $\Pi^* = 4\pi R_g^3\Pi/(3k_bT)$ ($\Pi^* = \pi R_g^2\Pi/(k_bT)$ and $\kappa \equiv \partial\Pi^*/\partial\sigma$ in the case of a two-dimensional system of tethered chains to a surface). Here Π, k_b, and T are the osmotic pressure, Boltzmann constant, and absolute temperature, respectively. The RPA excluded-volume interaction parameter can be related to a virial expansion of the reduced osmotic compressibility as $\kappa = 1 + 2A_2\Sigma + 3A_3\Sigma^2 + ... = 1 + 2A_2(\Sigma)\Sigma = 1 + \nu(\Sigma)$, where the $A_2(\Sigma) = A_2 + 3A_3\Sigma/2 + ...$ function defines the apparent second virial coefficient.[28] In the dilute limit the RPA expression reduces to the form factor of an ideal chain, while in the $q \to 0$ limit the inverse forward scattering is $F_{\mathrm{RPA}}^{-1}(q{=}0) = 1 + \nu = \kappa$, which is expected from a fluctuation dissipation theorem.

A block copolymer micelle consists of a diffuse corona of the dissolved block and a dense core of the insoluable block. The normalized form factor [$F_{\mathrm{micelle}}(q{=}0) = 1$] of a block copolymer micelle with a homogeneous spherical core can be written in terms of partial scattering contributions as

$$F_{\mathrm{micelle}}(q) = \frac{1}{(\beta_c + \beta_s)^2}[\beta_s^2\Phi^2(q) + \beta_c{}^2F_{\mathrm{cor}}(q) + 2\beta_s\beta_cA_{\mathrm{cor}}(q)\,\Phi(q)] \tag{3}$$

where the three contributions correspond to scattering from the core, the corona, and an interference term between the core and the corona, respectively. The corona and core excess scattering lengths are denoted β_c and β_s, respectively, and they are defined as $\beta_c = NV_c\Delta\rho_{\mathrm{chain}}$ and $\beta_s = NV_s\Delta\rho_{\mathrm{core}}$, where V_c, V_s, $\Delta\rho_{\mathrm{chain}}$, and $\Delta\rho_{\mathrm{core}}$ are the volume of a corona and core block, the excess scattering length densities of a corona block, and core block, respectively. A diblock copolymer micelle has implicitly been assumed, such that N denotes the aggregation number. In this paper the corona, core and corona−core interference contributions to the micelle scattering are normalized to unity in the $q \to 0$ limit. The normalized form factor amplitude of a sphere is given by Rayleigh[29] as $\Phi(qR_{co}) = 3[\sin(qR_{co}) - qR_{co}\cos(qR_{co})]/(qR_{co})^3$, where R_{co} is the radius of the micelle core.

Because the core is assumed to be spherical and homogeneous, A_{cor} only depends on the radial distribution of segments $\varphi(r)$, i.e., the corona profile, and A_{cor} will in the rest of the paper be denoted profile scattering.

It is given by

$$A_{\mathrm{cor}}(q) = \int_0^\infty \mathrm{d}r\; 4\pi r^2 \frac{\sin(qr)}{qr}\,\varphi(r) \tag{4}$$

If the single-chain scattering contribution is neglected as well as correlations due to density fluctuations caused by chain−chain interactions, the corona scattering is given by $F_{\mathrm{cor}} = A_{\mathrm{cor}}{}^2$. This is the approximation that yields a core−shell model of the micellar scattering,[30] which is the scattering from a configurationally averaged micelle, rather than the configurationally averaged scattering from a micelle, which is the scattering observed experimentally. As single-chain scattering is neglected, a core−shell model is unable to reproduce the characteristic single-chain power law decay at large q values, which is a signature of the chain connectivity, nor is a core−shell model able to represent the finite scattering observed in the minima where $A_{\mathrm{cor}}(q) = 0$. Only in the limit $\sigma \gg 1$ where the density of chains is very high, e.g. when the corona is in the brush regime, do we expect these fluctuations to be sufficiently suppressed for core−shell models to give a reasonable description.

For a micelle, the corona scattering is the sum of two contributions: a contribution from the intrachain scattering $F(q)$ (proportional to the number of chains N) and interchain scattering $H(q)$ (proportional to the number of different pairs of chains $N(N-1)$). The normalized $[F_{\mathrm{cor}}(q{=}0) = 1]$ corona scattering is thus given by

$$F_{\mathrm{cor}}(q) = \frac{F(q)}{N} + \frac{N-1}{N} H(q) \tag{5}$$

The separation of the corona scattering into interchain and intrachain scattering contributions is somewhat arbitrary. Another way of separating the corona scattering is in terms of the scattering from the configurationally averaged radial profile and from the correlations of the density fluctuations[31,32] about this average profile. The scattering due to the radial profile is given by $A_{\mathrm{cor}}{}^2$ as in a core−shell model. The density fluctuation correlation function depends on chain interactions and chain connectivity, and we model this by the scattering from a quasi-two-dimensional layer of dilute/semidilute solution using the RPA approximation:

$$F_{\mathrm{sol.prof}}(q) = \frac{F_{\mathrm{RPA}}(q)}{N} + \frac{N - F_{\mathrm{RPA}}(q{=}0)}{N} A_{\mathrm{cor}}{}^2(q) \tag{6}$$

Here the weighting of the two terms has been adjusted to account for the fact that scattering has been shifted from the profile scattering contribution into the fluctuation scattering contribution, and the fluctuation scattering contribution is not normalized. This expression for the corona scattering has separated the total scattering into a term that only depends on the scattering from a single chain and an excluded-volume parameter and a term that only depends on the radial profile of the corona and can be interpreted as being the scattering one would observed from a layer of polymer solution with a particular radial profile being confined to the micellar surface region. The first term of eq 6 is denoted the fluctuation scattering in the rest of this paper, while the second term is denoted profile scattering.

3. Monte Carlo Simulation

We have performed Monte Carlo (MC) simulations on block copolymer micelles.[33] Micelles were modeled as a spherical core with a number N of semiflexible chains tethered to it, where each chain consists of n bonds of length l_0. The valence angle between segments was fixed at 135.585°, which yielded a Kuhn length $b = 6l_0$ such that the semiflexible chain reproduces the radius of gyration of a flexible chain in the long-chain limit. The excluded-volume interaction was simulated by placing six hard spheres along each Kuhn length of the chain. The radius of the hard spheres was fixed at $0.1b$, which is known to reproduce the binary cluster integral of polystyrene in a good solvent.[35] The MC moves consisted of pivoting the individual chains,[36] and two surface MC moves, that moved and reorientated chains on the micelle surface. These were performed by pivoting the entire chain about the core center or the tether vertex, respectively. Configurations where a chain was found to overlap with other chains or the core region were rejected. We used the "zippering" algorithm[37] when checking for chain overlap, taking into account the semiflexibility of the chains, and taking care to avoid introducing local stiffness by allowing the hard spheres of neighboring vertexes along the chain to overlap. The initial micelle configuration was constructed using slightly stretched chains, which were grown while avoiding overlaps. This initially biased configuration was equilibrated by performing MC moves until the number of accepted moves was in excess of 100 times the number of degrees of freedom in the model. The three parameters controlling the step size of the MC moves were adjusted during the equilibration stage to yield approximately 50% acceptance probability for each of the three moves.

The chain was periodically reconstructed after every 50 000 pivot moves using the tabulated dihedral angles to avoid the buildup of numerical errors in the chain coordinate representation due to the many repeated rotations needed to sample the micellar configurations space. This reconstruction was made possible because each chain carries a virtual zeroth segment around with it, and the zeroth segment and the first segment, define a coordinate system in which it is easy to add another segment with a specific dihedral angle, valence angle, and segment length. This procedure, when iterated, uniquely reconstructs the chain based on a table of dihedral angles and a table which was created during chain formation and which was updated each time a pivot move was accepted. This is a cheap and effective operation compared to solving three linear equations for each segment as in the chain correction algorithm of Stellman and Gans[36] and also provides an easy way of creating the initial chain configuration. The deviation between the actual and expected dihedral angle was constantly below 3×10^{-12} during the simulation of the longest chain (229 segments), with deviations in segment length and valence angle below about a third of that. During a MC simulation the configuration was sampled for every 1000 attempted MC steps, and a simulation consisted of 100 blocks, each block being the average of 100 samples. Error bars were derived by analyzing the fluctuations of the block averages.

During MC simulations the radial density profiles $\varphi(R_j)$ were sampled in a number of bins at radii R_j as the number of vertexes lying in a spherical shell centered on the core with outer radius $(R_j + R_{j+1})/2$ and inner radius $(R_{j-1} + R_j)/2$. Each bin was normalized by

the volume of that spherical shell. We sampled the radius of gyration of the individual chains defined as

$$R_g^2 = \left\langle \frac{1}{(n+1)N} \sum_{i=1}^{N} \sum_{k=1}^{n+1} (\mathbf{R}_{cm,i} - \mathrm{r}_{ik})^2 \right\rangle \quad \text{with}$$

$$\mathbf{R}_{cm,i} = \frac{1}{n+1} \sum_{k=1}^{n+1} \mathbf{r}_{ik} \quad (7)$$

where $\mathbf{r}_{ik}$ is the position of the kth vertex on the ith chain. N is the number of chains, and $n + 1$ is the number of vertexes/scattering sites. The scattering from the micelle corona is given by the scattering from the set of vertexes and core as

$$F_{micelle}(q) \propto \langle |\beta_c \sum_{i=1}^{N} A_i + \beta_s \Phi|^2 \rangle \quad (8)$$

where the form factor amplitude of the ith chain is

$$A_i(\mathbf{q}) = \frac{1}{N(n+1)} \sum_{k=1}^{n+1} e^{i\mathbf{q}\cdot\mathbf{r}_{ik}} \quad (9)$$

Since the micelle core is assumed to be spherical and homogeneous, the core form factor amplitude Φ is real and can be moved outside the configurational and orientational average. The remaining configurational averages can be compared to the corresponding terms in eq 3. The normalized corona scattering and the profile scattering can be identified as

$$F_{cor}(q) = \frac{1}{N^2} \langle |\sum_{i=1}^{N} A_i|^2 \rangle \quad (10)$$

and

$$A_{cor}(q) = \frac{1}{N} \langle \mathrm{Re} \sum_{i=1}^{N} A_i \rangle \quad (11)$$

In this notation the single chain scattering and interchain scattering can be written as the sum of diagonal and off-diagonal members of eq 10 as

$$F(q) = \frac{1}{N} \langle \sum_{i=1}^{N} |A_i|^2 \rangle \quad \text{and}$$

$$H(q) = \frac{1}{N(N-1)} \langle \sum_{i \neq j}^{N} A_i A_j^* \rangle \quad (12)$$

Comparing these equations to eq 10 demonstrates the weighting used in the expression for corona scattering given by eq 5. The averages consist of a configurational as well as a orientational average. These were performed using MC sampling, and by evaluation of the scattering for 13 directions for each q value, and choosing a new set of random directions each time a block of 100 samples was completed. The set of q values were chosen as approximately logarithmic distributed but slightly tweaked such that many q values are the sum of two smaller q values or twice another q value. This converted many of the complex exponentials needed to evaluate eq 9 into simple products and squares of previously calculated complex numbers. This method of sampling yields a significant optimization of the time spend sampling the micellar scattering contributions.[33]

4. Results and Discussion

We have chosen a reference micelle defines as having $N = 44$ chains, chain length $L = 8.33b$, and core radius $R_{co} = 3.33b$, as this mimics the configuration of the Pluroic P85 micelles.[34] We use the Kuhn length b as a length scale. We have performed three series of simulations where one of the parameters N, L, and R_{co} was varied while keeping the remaining two fixed at their reference values. The range of variation was chosen to correspond to a variation of surface coverage in the range from 0.01 to 5, covering the experimentally accessible regime for copolymer micelles.[2,16,17]

Figure 1 shows the corona scattering for simulations where the number of chains is varied. A qualitative examination shows a huge decrease of scattering at high q values relative to the scattering at low q values as the number of chains is increased, while the amplitude of the first subsidiary oscillation increases and higher-order oscillations progressively become more pronounced. This is caused by the weighting between the highly oscillatory interchain scattering $H(q)$ and the nonoscillatory intrachain scattering $F(q)$. The scattering is dominated by single-chain scattering and its $1/N$ dependence at high q values, while the rapidly decaying profile scattering contribution dominates at low q values. The minima of the corona scattering correspond to q values where $A_{cor}(q) = 0$, and in those minima the scattering intensity is given solely by the fluctuation scattering F_{RPA}.

Figure 2 shows the corona scattering corresponding to simulations where the core radius is decreased for fixed number of chains and core radius. Decreasing the core radius causes the oscillations due to the radial profile to shift toward larger q values. Simultaneously, the oscillations are reduced as the interchain scattering becomes progressively less dominant compared to the chain scattering $F(q)$, which is essentially unchanged by a decrease in core radius.

The logarithm of the absolute value of the profile scattering is shown in Figures 3 and 4. Each sign change gives rise to an inverted peak due to the logarithm. A qualitative examination shows that increasing the number of chains has only a slight effect on the profile scattering i.e., the corona profile, as the first inverted peaks are shifted slightly toward smaller q values, indicating a slight increase of the corona width. When the core radius is decreased, a huge shift is seen in the shift of the oscillations toward larger q values shown in Figure 4, which indicates that varying core radius has a large impact on the corona profile. Simulations where the chain length is increased will display similar effects as those where the core radius is decreased, as this provides two opposite mechanisms of controlling the surface curvature, which can be quantified by the dimensionless ratio of the radius of gyration to core radius. A broadening of the first subsidiary and second subsidiary oscillation is observed in Figures 3 and 4, and this is attributed to effects of surface coverage and surface curvature on the shape of the corona profile.

Figure 5 shows the reduced density profiles sampled during the simulations, where the number of chains or core radius was varied. Simulations varying the chain length yields the same reduced density profile as simulations varying the core radius, as these simulta-

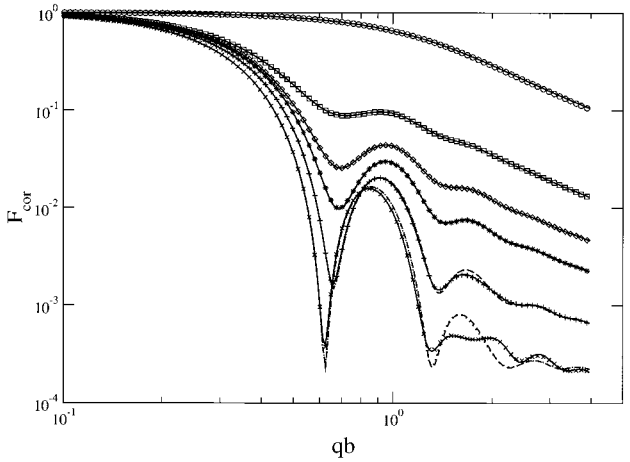

Figure 1. Corona scattering for simulations varying the number of chains corresponding to surface coverages $\sigma = 0.016$, 0.13, 0.36, 0.72, 2.15, and 5.37 (top to bottom using symbols). Lines are model fits. Dotted line: BoxGauss; dashed line: ME2; and solid line: ME3 profile.

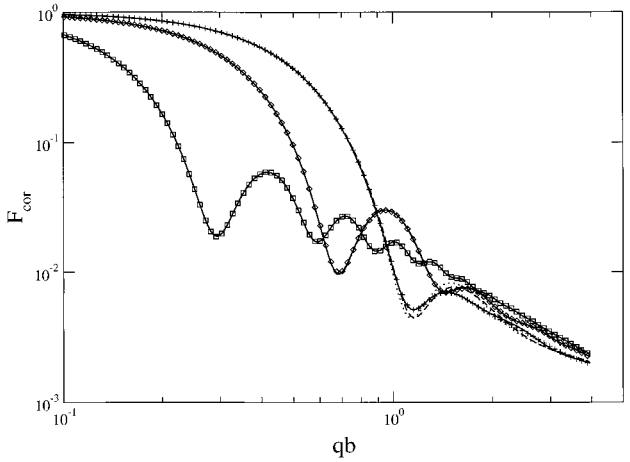

Figure 2. Corona scattering for simulations varying the core radius corresponding to surface coverages $\sigma = 0.13$, 0.72, and 2.10, respectively (using box, diamond, and plus symbols, respectively). Lines are model fits. Dotted line: BoxGauss; dashed line: ME2; and solid line: ME3 profile.

neously varies the surface coverage and curvature in a similar manner. The reduced density profiles are defined as $\varphi'(r') = \varphi(r')/C$ where $C = \int\varphi(r')\,dr'$ is a normalization constant, and the reduced radius is defined as $r' = (r - R_{co})/(\langle r\rangle - R_{co})$, where $\langle r\rangle = \int r\varphi(r)4\pi r^2\,dr$ is the first moment of the simulated profile. This representation shows the change of the profile shape rather than the change of the profile itself.

At low surface coverage all profiles indicate a depletion zone close to the core; however, no depletion zone is present when the surface coverage is increased above unity. At sufficiently large surface curvatures the $\varphi(r) \propto r^{-4/3}$ scaling behavior predicted by Halperin[38] is clearly observed in the vicinity of the core surface; however, further away from the core the radial profiles decay faster than predicted by Halperin, which is due to the finite length of the simulated chains. Upon variation of the number of chains, the profile only shows a dependence on the number of chains for surface coverages above unity, indicating that chain interactions are negligible for surface coverages below unity. The profile for simulations where the chain length is varied shows a large change of shape. This is due to the fact that the

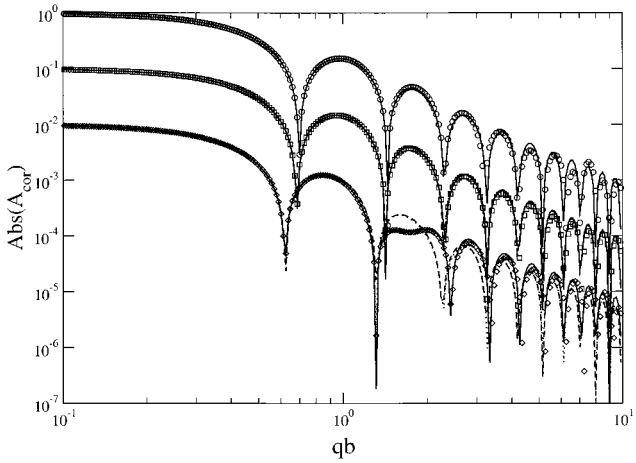

Figure 3. Profile scattering for simulations varying the number of chains corresponding to surface coverages $\sigma = 0.016$, $\sigma = 0.72$ (shifted down 1 decade), and $\sigma = 5.37$ (shifted down 2 decades). Lines are model fits using BoxGauss profile (dotted), ME2 profile (dashed line), and ME3 profile (solid line).

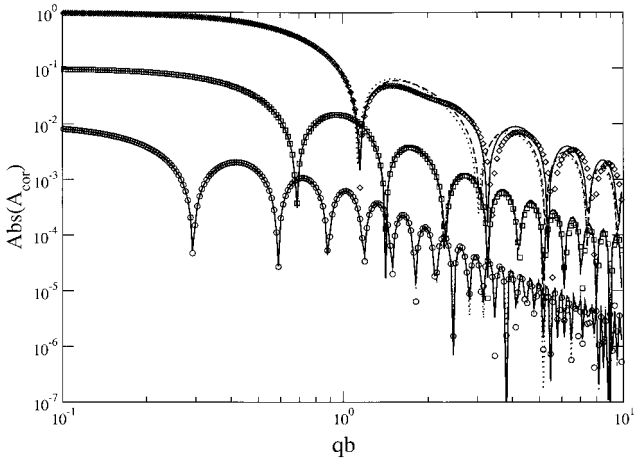

Figure 4. Profile scattering for simulations varying the core radius corresponding to surface coverages $\sigma = 0.13$ (shifted down 2 decades), $\sigma = 0.72$ (shifted down 1 decade), and $\sigma = 2.10$. Lines are model fits using BoxGauss profile (dotted), ME2 profile (dashed line), and ME3 profile (solid line).

effective surface curvature R_g/R_{co} is simultaneously increased in this case.

5. Analysis and Modeling of the Results

For a quantitative analysis of the simulated scattering, two parameters are required for the fluctuation scattering, namely the radius of gyration R_g and the excluded-volume parameter in the RPA expression, which is assumed to be a function of the surface coverage $\nu(\sigma)$. We have assumed that the excluded-volume coefficient only depends on the reduced surface coverage, in analogy with an ordinary polymer solution where it is a function of the reduced density Σ as shown in the theory section. We have simulated semiflexible chains, as this provides a relatively realistic model for real polymer chains. The simple RPA expression is modified using a Daniels form factor in the denominator,[39] which takes the semiflexibility of the chains into account in an approximate manner, while we retain the Debye form factor in the numerator of the RPA expression. Simulations have shown that this provides a quite accurate expression for the scattering from semidilute

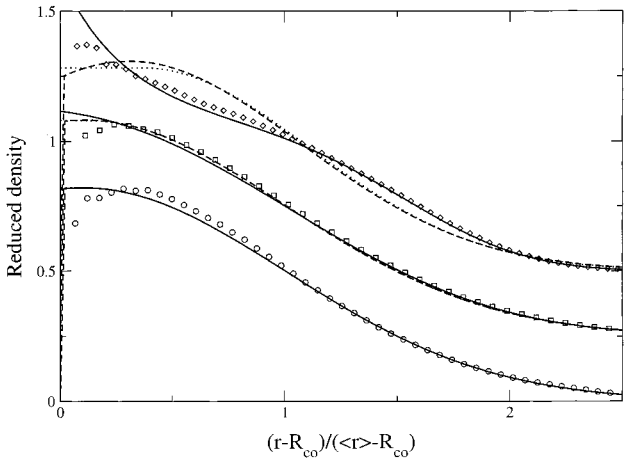

Figure 5. Reduced radial density profiles obtained from simulations varying number of chains (symbols) and profiles obtained by fitting the scattering using the BoxGauss (dotted lines), ME2 (dashed lines), and ME3 profile (solid line). The fitted profiles have been transformed using the parameters as for the simulation profile. Simulation profiles are shown for a number of chains corresponding to surface coverages $\sigma = 0.05$ (circle), $\sigma = 0.72$ (box shifted up 0.25), and $\sigma = 5.37$ (diamond, shifted up 0.5).

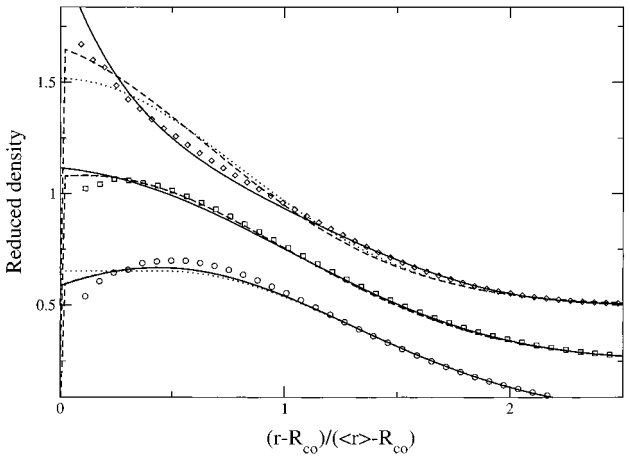

Figure 6. Reduced radial density profiles obtained from simulations varying the core radius (symbols) and profiles obtained by fitting the scattering using the BoxGauss (dotted lines), ME2 (dashed lines), and ME3 profile (solid line). The fitted profiles have been transformed using the parameters for the simulation profile. Simulation profiles are shown for a core radius corresponding to surface coverages $\sigma = 0.13$ (circle), $\sigma = 0.72$ (box, shifted up 0.25), and $\sigma = 2.10$ (diamond, shifted up 0.5).

solutions of semiflexible polymers.[40] The full expression for the fluctuation scattering contribution is

$$F_{\mathrm{RPA}}(qR_g) = \frac{F_{\mathrm{Daniels}}\left(\frac{q^2 R_g^{\,2}}{e(L/b)}\right)}{1 + \nu(\sigma) F_{\mathrm{Debye}}(q^2 R_g^{\,2})} \tag{13}$$

$$F_{\mathrm{Daniels}}(x) = F_{\mathrm{Debye}}(x) + \frac{b}{15L}(4 + 7x^{-1} - (11 + 7x^{-1})\mathrm{e}^{-x})$$

$$F_{\mathrm{Debye}}(x) = \frac{2[x - 1 + \exp(-x)]}{x^2}$$

and

$$e(n) = 1 - \frac{3}{2n} + \frac{3}{2n^2} - \frac{3}{4n^3}(1 - \mathrm{e}^{-2n})$$

Here $e(n)$ is a correction to the radius of gyration of the Daniels expression due to the finite number of statistically independent segments in our simulations.[41] The profile scattering A_{cor} is the Fourier transform of the radial profile and requires an expression for the radial monomer profile $\varphi(r)$. To our knowledge, no theoretical expressions exist for the radial density profiles of spherical micelles in the low to medium coverage limit, which we explore in the present paper. As a result, we use three empirical profiles, all of which are generalizations of a Gaussian distribution.

The first profile we use is a box with a Gaussian tail, abbreviated BoxGauss profile, which is defined as follows:

$$\varphi(r) = \begin{cases} 0 & r < R_{\mathrm{co}} \\ B & R_{\mathrm{co}} \le r < R_{\mathrm{ch}} \\ B \exp[-(r - R_{\mathrm{ch}})^2/(2s^2)] & R_{\mathrm{ch}} \le r \end{cases}$$

Here $B^{-1} = \int \varphi(r) 4\pi r^2 \, \mathrm{d}r$ is a normalization constant, R_{ch} is the outer edge of the box, and s defines the length scale on which the Gaussian tail decays. The normalized scattering from this profile is given by

$$A_{\mathrm{cor}}(q,s,R_{\mathrm{ch}}) = \frac{V_g(R_{\mathrm{ch}},s)\, S_g(q,R_{\mathrm{ch}},s) + V(R_{\mathrm{ch}})\, \Phi(qR_{\mathrm{ch}}) - V(R_{\mathrm{co}})\, \Phi(qR_{\mathrm{co}})}{V_g(R_{\mathrm{ch}},s) + V(R_{\mathrm{ch}}) - V(R_{\mathrm{co}})} \tag{14}$$

Here $\Phi(qR)$ is the normalized form factor amplitude for a homogeneous sphere with a volume $V(R) = 4\pi R^3/3$, and the normalized scattering contribution of the half-Gaussian is

$$S_g(q,r,s) = \{qr(4rs + \sqrt{2\pi}(r^2 + s^2))\}^{-1}\Big\{2rs \sin(qr) + \sqrt{2\pi}\exp\Big(-\frac{(qs)^2}{2}\Big)(qrs^2 \cos(qr) + r^2 \sin(qr)) + 2\sqrt{2}D\Big[\frac{qs}{\sqrt{2}}\Big](r^2 \cos(qr) - qrs^2 \sin(qr))\Big\}$$

while the corresponding volume of the half-Gaussian profile is

$$V_g(r,s) = 2\pi s(4rs + \sqrt{2\pi}(r^2 + s^2))$$

The Dawson integral is given by $D[y] = \exp(-y^2) \int_0^y \exp(t^2)\, \mathrm{d}t$, and a numerical expression for this integral is given in Numerical Recipes.[46] An expression for the scattering from a Gaussian-shaped profile has previously been reported by Bagger-Jörgensen et al.;[42] however, the published expression contains errors.

We also use two maximum entropy (ME)[20−22] profiles for analyzing the data. These profiles are based on the assumptions that no chains enter the micellar core, such that $\varphi(r) = 0$ for $r < R_{\mathrm{co}}$. We furthermore assume knowledge of the first two or three momenta of the

profile. In general, assuming knowledge of the first m momenta of profile leads to an entropy functional

$$S[\varphi] = \int_{R_{co}}^{\infty} \mathrm{d}r\, 4\pi r^2 \varphi(r)(-K \ln \varphi(r) + \sum_{n=0}^{m} \lambda_n r^n)$$

where a uniform prior is assumed. Here λ_n is a set of Lagrange multipliers to ensure the $m + 1$ constraints of the momenta of the distribution $\varphi(r)$. The zeroth constraint ensures normalization. Upon variation of the entropy functional it is seen that the maximum entropy profile can be written as

$$\varphi^m(r; a_1, ..., a_m) = \begin{cases} 0 & r < R_{co} \\ B \exp[-\sum_{n=1}^{m} a_n (r - R_{co})^n] & r \geq R_{co} \end{cases}$$

where B is a normalization constant, and the set of a_n's are related to the Lagrange multipliers. We take these as fit parameters when fitting the scattering. For $m = 2$ the normalized profile scattering produced by this profile, hence denoted the ME2 profile, can be worked out for $a_2 > 0$. This yields

$$A_{cor}(q,a_1,a_2) = [4{a_2}^{3/2} \sin(qR_{co}) + 2a_2\sqrt{\pi}\mathrm{Re}\{\mathrm{Erfc}(x + iy) \exp(x^2 - y^2)(q + ib)\mathrm{e}^{ic}\}]/ [\sqrt{\pi}(2a_2 + b^2)q\, \mathrm{Erfc}(x) \exp(x^2) - 2\sqrt{a_2}(a_1 - 4a_2R_{co})q] \quad (15)$$

where $b = 2a_2R_{co} - a_1$, $c = 2xy - qR_{co}$, $x = a_1/(2\sqrt{a_2})$, and $y = q/(2\sqrt{a_2})$. $\mathrm{Re}\{z\}$ is the real part of the complex number z, and $\mathrm{Erfc}(z)$ is the complementary error function of complex argument; an expression for $\mathrm{Erfc}(x + iy) \exp(x^2 - y^2)$ is also given in the Appendix. In the limit of $R_{ch} \rightarrow R_{co}$ and $a_1 \rightarrow 0$ both profiles converges toward a simple Gaussian profile, and the two scattering expressions given by eqs 14 and 15 are identical.

We have also used a ME profile with $m = 3$ denoted the ME3 profile. The profile scattering was obtained by numerical Fourier transformation of the profile. The profile was represented by 500 piecewise linear segments in the range from R_{co} to $R_{co} + 6R_g$, and an analytical expression for the Fourier transform was used for the scattering from each segment.

The corona and profile scattering obtained from the MC simulations using eqs 10 and 11 were fitted simultaneously by the corresponding theoretical expressions given by eqs 6 and 4, where we model the fluctuation scattering by eq 13, and we model the profile by one of the three profiles: box with a Gaussian tail (abbreviated BoxGauss) and a maximum entropy profile assuming knowledge of the first two or three momenta (abbreviated ME2 and ME3). The fit parameters for the fluctuation scattering are the radius of gyration R_g and the excluded-volume coefficient ν. The fit parameters for the radial profiles are R_{co} and s for the BoxGauss profile, while the first two or three a_n parameters are fitted for the two ME profiles. The fit range for the profile scattering was $qb < 10$ and $qb < 4$ for the corona scattering. The latter range is dictated by the fact that the Daniels expression is not valid for larger values of qb, as it fails to reproduce the rigid rod scattering behavior observed at large q values.

The results of fitting the model using the three profiles to the simulation results for the corona scattering and profile scattering are shown in Figures 1−4. For $\sigma < 1$ all the fits have reduced chi-square value[43] ${\chi_{red}}^2 < 5$, except for the simulations with the shortest chains $L = 2b$ and $L = 4b$ which have a ${\chi_{red}}^2 < 30$. These large values are due to the fact that the Daniels distribution is not valid for chains with so few statistical segments. In the $\sigma < 1$ range the ME2 and ME3 profiles are identical since the a_3 parameter is estimated to zero within the statistical errors for the ME3 profile. For simulations with very large core radii both ME fits consistently have somewhat smaller ${\chi_{red}}^2$ values compared to the BoxGauss profile fits; however, for simulations with a low aggregation number, all three profiles provide fits of similar quality. The agreement between model and simulation data is excellent for surface coverage $\sigma < 1$ for all three profiles. However, for $\sigma > 1$ the fits provided by the ME2 profile are comparable to those using the BoxGauss profile, while the ME3 profile consistently provides significantly better fits, yielding reductions in ${\chi_{red}}^2$ of at least an order of magnitude. This vast improvement can be understood by observing the deviations shown in the high q part of corona scattering shown in Figures 1 and 2 for the largest surface coverage. These deviations are caused by the inability of the profile in representing the actual profile scattering, as shown in Figures 3 and 4, where the ME3 profile can be seen to give a much better fit to the profile scattering compared to the BoxGauss and ME2 profiles.

Profiles obtained by fitting the scattering and profiles sampled during the simulation are shown in Figures 5 and 6. They have been plotted using the scaling transformation of the corresponding simulation profile to avoid introducing artifacts when comparing the two scaled profiles. For low surface coverages the fitted profiles are very similar and show a good agreement with the simulated profiles. For high surface coverages the ME3 profile give significantly better estimates than the two other profiles. These deviations at high surface coverages are reflected in the deviations in the profile scattering shown in Figures 3 and 4. The deviations in the vicinity of the core do not appear to have any effect on the profile scattering.

For $\sigma < 1$ fitting the three profiles yields identical estimates of the radius of gyration and the excluded-volume parameter, while for $\sigma > 1$ significant deviations are observed between the estimates provided by fitting the three model expressions. These are caused by the inability of the BoxGauss and ME2 profiles in fitting the sampled profile scattering and corona scattering at high q values. Both the radius of gyration and the excluded-volume parameter are estimated from the corona scattering at high q values, and as a result of this we only report the results obtained from the fits using the ME3 profile.

The radius of gyration obtained from the simulations is shown in Figure 7. The simulations where the surface coverage is increased by increasing the number of chains or decreasing the core radius have a radius of gyration with a similar dependence on surface coverage. The radius of gyration estimated by the fits is also shown, and they are in good agreement with the simulations results with less than 2% deviation for simulations with a low number of chains or large core radius. Larger deviations (12% for the highest surface coverage) are apparent for simulations with long chains.

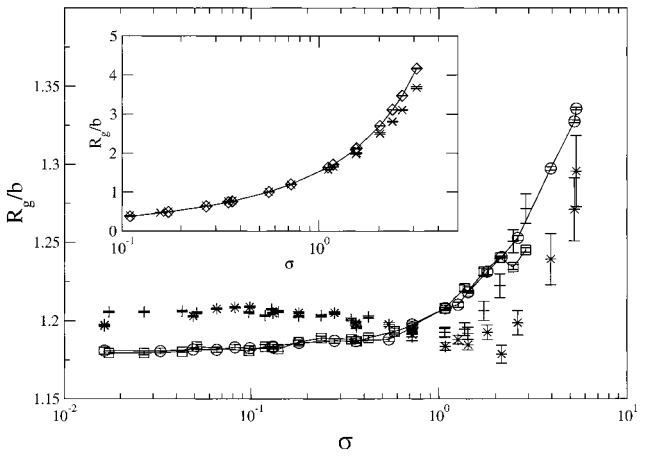

Figure 7. Radius of gyration obtained from simulation (lines and symbols) and from fits (symbols) varying number of chains (circle and line) and core radius (box and line). The inset shows the radius of gyration for simulations varying chain length (diamond and line). Radius of gyration estimated by fitting the scattering using the ME3 profile for simulations varying the number of chains (star), core radius (plus), and chain length (cross).

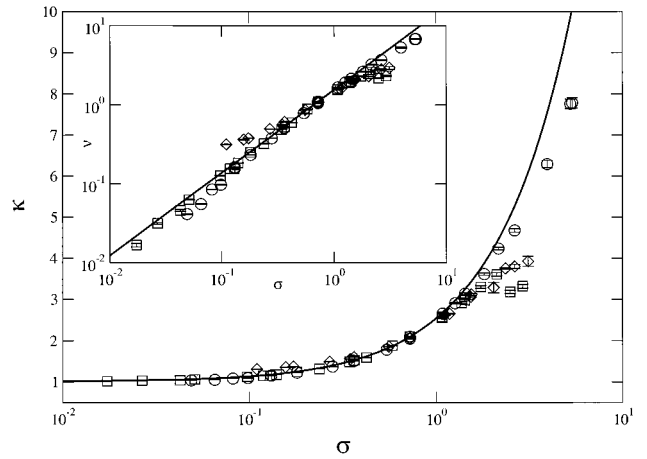

Figure 8. Compressibility κ vs surface coverage σ obtained from fitting the ME3 profile to the simulation data. Inset shows the excluded-volume coefficient $\nu(\sigma)$ plotted against surface coverage for fits using the ME3 profile. Simulations varying number of chains (circle), core radius (diamond), and chain length (box). The solid line in the inset is the power law relation $\nu(\sigma) = 1.42\sigma^{1.04}$, and the solid line is the corresponding compressibility.

The inset in Figure 8 shows the $\nu(\sigma)$ parameters obtained from fits using the ME3 profile. While this parameter also depends on the surface coverage and the number of chains, the points from simulations varying number of chains, core radius, and chain length collapse on the same curve, which shows a power law dependence on surface coverage. The power law is $\nu(\sigma) = \alpha\sigma^{\beta}$ with $\alpha = 1.42 \pm 0.03$ and $\beta = 1.04 \pm 0.02$. The simulations with the shortest chains can be observed to deviate from this behavior, which we attribute to the Daniels form factor not being valid for such short chains. Previously, we have analyzed the scattering data using a self-consistent approach,[44] where the single-chain scattering, sampled using eq 12 during MC simulations, was used in numerator and denominator in the RPA expression given by eq 13. $\nu(\sigma)$ was derived by equating eqs 5 and 6 in the first minima of the profile scattering where $A_{cor}(q) = 0$, and a power law behavior with $\alpha = 1.35 \pm 0.02$ and $\beta = 0.95 \pm 0.02$ was found. This indicates that while $\nu(\sigma)$ shows a simple power law relation on σ, the corresponding constant and exponent shows a weak dependence on the particular expressions used for the chain and profile scattering.

The forward scattering due to density fluctuations is related to the reduced osmotic compressibility κ through a fluctuation dissipation theorem, which states that the osmotic compressibility is inversely proportional to the $q \rightarrow 0$ limit of the Fourier transform of the density fluctuation correlation function. For a polymer solution the observed scattering is due to density fluctuations, and as a result it is easy to obtain the osmotic compressibility by extrapolating the observed scattering to the $q \rightarrow 0$ limit. For a micellar corona the scattering at low q values is dominated by profile scattering due to the average radial profile. Thus, the profile scattering dominates the scattering due to the density fluctuations, making a simple extrapolation impossible; however, by modeling the profile and fluctuation scattering separately as we have done in this paper, it is trivial to obtain the $q \rightarrow 0$ limit of the fluctuation scattering contribution as $F^{-1}_{RPA}(q{=}0) = \kappa = 1 + \nu(\sigma)$ just as for a polymer solution.[24] The reduced osmotic compressibility is shown in Figure 8 and can be seen to follow a universal dependence on the surface coverage except for high surface coverages where deviations due to a dependence on the number of chains and surface curvature can be seen.

6. Conclusions

We have presented Monte Carlo simulation results performed on the scattering from a micelle as a function of number of chains, chain length, and core radius. We have, furthermore, presented novel empirical model expressions for the scattering from block copolymer micelles with a spherical core and that includes the effects of excluded-volume interactions. The corona scattering is represented as a sum of scattering contributions due to the average radial density profile and the density fluctuations correlations about this profile. We model the fluctuation contribution to the scattering as that of a dilute/semidilute polymer solution. The proposed model depends on the radius of gyration, an excluded-volume parameter, which is proportional to the apparent second virial coefficient, and an expression for the radial profile of the micellar corona. To our knowledge, there is no theoretical expression available for the radial profile except in the high curvature limit. We used three empirical expressions for the corona profile: one with a box with a Gaussian tail and two maximum entropy estimates where knowledge of the two or three first momenta was assumed. The model expressions for the corona scattering and profile scattering were simultaneously fitted to the scattering obtained directly from the MC simulations. These fits show an excellent agreement for low surface coverages $\sigma < 1$ for all three profiles, while the ME3 profile shows an excellent agreement also for $\sigma > 1$, where the BoxGauss and the ME2 profile show significant deviations at high q values for the corona scattering. These deviations are caused by the fact that the BoxGauss and ME2 profiles provide a poor represention of the actual corona profile. This is reflected in the estimates of radius of gyration and the excluded-volume parameter by these two models, as these are estimated from the high-q behavior of the

corona scattering where the fluctuation scattering dominates. For $\sigma < 1$ all profiles provide identical estimates for the radius of gyration and excluded-volume parameter. Besides providing estimates for the radius of gyration and the excluded-volume parameter, the fits also provide estimates for the radial profile, which can be compared to the actual radial profiles obtained from the MC simulation.

Profiles obtained by fitting the simulated scattering are in good agreement with the profiles obtained directly from simulations, except for small deviations close to the core. For $\sigma < 1$ the three profiles obtained from the fits of the simulated scattering are very similar; however, at high surface coverages, the ME3 profile yields a significantly better estimate for the radial profile. The simulated model has a sharp core−corona interface in contrast to the diffuse interface expected for real micellar systems; however, this is easy to include in the profile scattering expression, either by directly modifying the radial profile or by multiplying the scattering with a Debye−Waller factor as $A_{cor}(q) \rightarrow \exp(-q^2d^2/2)A_{cor}(q)$ to account for a diffuse corona−core interface.[47]

The fits yields estimates of the radius of gyration that are in good agreement with the radius of gyration obtained directly from simulations. Plotting the excluded-volume parameter against reduced surface coverage for simulations varying chain length, number of chains, and core radius shows that the results approximately fall on a common curve corresponding to a power law behavior. However, the coefficients and exponents are slightly different from those we have previously obtained through a self-consistent analysis, where simulation results for the single chain scattering were used in the RPA expression for the corona scattering, thus forming a completely self-consistent expression for the corona scattering. This suggests that the power law behavior is sensitive to the model expressions used for fitting the scattering.

We have shown that the effects from chain connectivity and excluded-volume interactions between tethered chains on the scattering of a micelle with a spherical core can be described by a relatively simple model, where the corona is modeled as a dilute/semidilute solution with a particular radial profile. We note that this method of including connectivity and excluded-volume interactions effects in the scattering from colloidal aggregates can be generalized to geometries such as micelles with elliptical and cylindrical cores. The models of the scattering from colloidal aggregates presented in the present paper allow more accurate and detailed information to be obtained from the analysis of experimental results. We are currently applying the expressions in the analysis of small-angle neutron contrast variation data and small-angle X-ray scattering data for micelles of polystyrene−polyisoprene in decane. These results along with modifications of the scattering expressions to account for diffuse core−corona interfaces and structure factor effects on the micellar scattering will be presented in a future article.[48]

Appendix

The real and imaginary parts of $G(x,y) = \exp(x^2 - y^2)\mathrm{Erfc}(x + iy)$ can be separated into real and imaginary parts using an infinite series approximation[45]

$$G(x,y) = e^{x^2-y^2}\,\mathrm{Erfc}(x) - \frac{e^{-y^2}}{2\pi x}\cos(2xy) - \frac{2}{\pi}\sum_{n=1}^{\infty}\frac{e^{-n^2/4-y^2}}{n^2+4x^2}f_n(x,y) + i\left\{-\frac{e^{-y^2}\sin(2xy)}{2\pi x} - \frac{2}{\pi}\sum_{n=1}^{\infty}\frac{e^{-n^2/4-y^2}}{n^2+4x^2}g_n(x,y)\right\}$$

where

$$f_n(x,y) = 2x - 2x\cosh(ny)\cos(2xy) + n\sinh(ny)\sin(2xy)$$

$$g_n(x,y) = 2x\cosh(ny)\sin(2xy) + n\sinh(ny)\cos(2xy)$$

Here $\mathrm{Erfc}(x)$ is the real complementary error function. An expression for it is given in Numerical Recipes.[46] Evaluation of the two auxiliary functions f_n and g_n can be optimized using the addition formulas in which case only $\cosh(y)$ and $\sinh(y)$ need to be evaluated, and subsequent evaluations of $\cosh(ny)$ and $\sinh(ny)$ require only a few simple arithmetic operations of precalculated constants.

References and Notes

(1) Mortensen, K.; Pedersen, J. S. *Macromolecules* **1993**, *26*, 805.
(2) McConnell, G. A.; Lin, E. K.; Gast, A. P.; Huang, J. S.; Lin, M. Y.; Smith, S. D. *Faraday Discuss.* **1994**, *98*, 121.
(3) Gast, A. P. *Langmuir* **1996**, *12*, 4060.
(4) Szleifer, I.; Carignano, M. A. *Adv. Chem. Phys.* **1996**, *94*, 165.
(5) Halperin, A.; Tirrell, M.; Lodge, T. P. *Adv. Polym. Sci.* **1992**, *100*, 31.
(6) Carignano, M. A.; Szleifer, I. *J. Chem. Phys.* **1993**, *98*, 5006.
(7) Carignano, M. A.; Szleifer, I. *Macromolecules* **1995**, *28*, 3197.
(8) Carignano, M. A.; Szleifer, I. *J. Chem. Phys.* **1994**, *100*, 3210.
(9) Netz, R. R.; Schick, M. *Macromolecules* **1998**, *31*, 5105.
(10) Li, H.; Witten, T. A. *Macromolecules* **1994**, *27*, 449.
(11) Dan, N.; Tirrell, M. *Macromolecules* **1992**, *25*, 2890.
(12) Wijmans, C. M.; Zhulina, E. B. *Macromolecules* **1993**, *26*, 7214.
(13) Toral, R.; Chakrabarti, A. *Phys. Rev. E* **1993**, *47*, 4240.
(14) Murat, M.; Grest, G. S. *Macromolecules* **1991**, *24*, 704.
(15) Adamuti-Trache, M.; McMullen, W. E.; Douglas, J. F. *J. Chem. Phys.* **1996**, *105*, 4798.
(16) Derici, L.; Ledger, S.; Mai, S.-M.; Booth, C.; Hamley, I. W.; Pedersen, J. S. *Phys. Chem. Chem. Phys.* **1999**, *1*, 2773.
(17) Pedersen, J. S.; Hamley, I. W.; Ryu. C. Y.; Lodge. T. P. *Macromolecules* **2000**, *33*, 542.
(18) de Gennes P. G. *C. R. Acad. Paris, Ser.* II **1986**, *302*, 765.
(19) Farago, B.; Monkenbusch, M.; Richter, D.; Huang, J. S.; Fetters L. J.; Gast, A. P. *Phys. Rev. Lett.* **1993**, *71*, 1015.
(20) Gilmore, C. J. *Acta Crystallogr.* **1996**, *A52*, 561.
(21) Bricogne, G. *Acta Crystallogr.* **1984**, *A40*, 410.
(22) Jaynes, E. T. *Phys. Rev.* **1957**, *106*, 620.
(23) Debye, P. *J. Phys. Colloid Chem.* **1947**, *51*, 18.
(24) Daoud, M.; Cotton, J. P.; Farnoux, B.; Jannink, G.; Sarma, G.; Benoit, H.; Duplessix, R.; Picot, C.; de Gennes, P. G. *Macromolecules* **1975**, *8*, 804.
(25) de Gennes, P. G. *Scaling Concepts in Polymer Physics;* Cornell University Press: Ithaca, NY, 1979.
(26) Schweizer, K. S.; Curro, J. G. *Adv. Polym. Sci.* **1994**, *116*, 319.
(27) Fuchs, M.; Müller, M. *Phys. Rev. E* **1999**, *60*, 1921.
(28) Benoit, H.; Benmouna, M. *Polymer* **1984**, *25*, 1059.
(29) Lord Rayleigh *Proc. R. Soc. London* **1911**, *A84*, 25.
(30) Förster, S.; Burger, C. *Macromolecules* **1998**, *31*, 879.
(31) Auvray, L.; de Gennes, P. G. *Europhys. Lett.* **1986**, *2*, 647.
(32) Cosgrove, T.; Heath, T. G.; Ryan, K.; Crowley, T. L. *Macromolecules* **1987**, *20*, 2879.
(33) Svaneborg, C.; Pedersen, J. S. *J. Chem. Phys.* **2000**, *112*, 9661.
(34) Pedersen, J. S.; Gerstenberg, M. C. *Macromolecules* **1996**, *29*, 1363.
(35) Pedersen, J. S.; Schurtenberger, P. *Macromolecules* **1996**, *29*, 7602.
(36) Stellman, S. D.; Gans, P. J. *Macromolecules* **1972**, *5*, 516.

(37) Stellman, S. D.; Froimowitz, M.; Gans, P. J. *J. Comput. Phys.* **1971**, *7*, 178.
(38) Halperin, A. *Macromolecules* **1987**, *20*, 2943.
(39) Burchard, W.; Kajiwara, K. *Proc. R. Soc. London* **1970**, *A316*, 185.
(40) Pedersen, J. S.; Schurtenberger, P. *Europhys. Lett.* **1999**, *45*, 666.
(41) Benoit, H.; Doty, P. *J. Phys. Chem.* **1953**, *57*, 958.
(42) Bagger-Jörgensen, H.; Olsson, U.; Mortensen, K. *Langmuir* **1997**, *13*, 1413.
(43) Pedersen, J. S. *Adv. Colloid Interface Sci.* **1997**, *70*, 171.
(44) Svaneborg, C.; Pedersen, J. S. *Phys. Rev. E: Rapid Commun.* **2001**, *63*, 10802.
(45) Abramowich, M.; Stegun, I. A *Handbook of Mathematical Functions;* Dover: Mineola, NY, 1965; eq 7.1.29.
(46) Press, W. H.; Teukolsky, S. A.; Vetterling, W. T.; Flannery B. P. *Numerical Recipes*; University Press: Cambridge, 1992.
(47) Pedersen, J. S. Structural Studies by Small-Angle Scattering and Specular Reflectivity. Risø Report Risø-R-1166(EN), 1999; p 51. Available on request from The Information Service Department, Risø National Laboratory, DK-4000 Roskilde, Denmark.
(48) Pedersen, J. S.; Svaneborg, C.; Almdal, K.; Hamley, I. W.; Young, R. N., in preparation.

MA011046V